Active Ferromagnetic Metasurface with Topologically Protected Spin Texture for Spectral Filters

Haiming Yu, Jilei Chen, Vincent Cros, Paolo Bortolotti, Hanchen Wang, Chenyang Guo, Florian Brandl, Florian Heimbach, Xiufeng Han, Abdelmadjid Anane, and Dirk Grundler*

Electromagnetic metasurfaces modulate a material's response to electromagnetic waves by specifically arranged elements with dimensions below the wavelength. They have opened new fields of research, including flat optics and nanophotonics on a chip. Ferromagnetic metasurfaces could become the building blocks for manipulation of both microwaves and spin waves (magnons). So far, the functionality of magnonic devices has been limited by high intrinsic damping of the materials employed, suppressing long-distance spin-wave propagation. Here ferromagnetic metasurfaces are reported, which are created from periodic arrays of either 15 nm thick $Co_{20}Fe_{60}B_{20}$, $Ni_{80}Fe_{20}$ or Co nanodisks on ferrimagnetic yttrium iron garnet (YIG) hosting topologically protected vortex states. This device, a reconfigurable spectral filter, operates in the microwave regime near 0.9 GHz and manipulates long-distance spin-wave transmission in thin YIG. An efficiency of 98.5% is demonstrated, with the metasurface covering only 15% of the microwave antenna. This first demonstration of a ferromagnetic metasurface opens unprecedented possibilities for on-chip control of microwaves in low-damping ferrimagnetic insulators.

1. Introduction

Metasurfaces are 2D planar nanostructured interfaces which are used to manipulate the electromagnetic waves in amplitude,

phase and polarization.[1–5] Applications of metasurfaces such as spectral filters, perfect transmitters and perfect absorbers are explored for optics,[1–5] plasmonics,[6] acoustic waves,[7] and microwaves.[8] They provide efficient control of reflected and transmitted waves.[9–11] Building blocks of photonic metasurfaces are usually made from metallic or dielectric sub-wavelength nanoelements[12] with thicknesses between about 20 and several 100 nm.[1] A missing brick in the 2D metasurface family is the metasurface prepared from magnetically ordered materials (ferro-, ferri-, and antiferromagnets). When microwaves are introduced into such magnetic systems, they couple to the spins and cause uniform and non-uniform spin precession, that is, ferromagnetic resonance at wavevector $k = 0$ and spin waves with $k \neq 0$, respectively. For realizing the functionality of the microwave spectral filtering, different concepts could be applied such as microwave lumped elements,[13] mechanical engineering by the kirigami technique,[14] and metasurfaces composed of metallic and dielectric layers.[15] Ferromagnetic

H. Yu, J. Chen, H. Wang, F. Heimbach
Fert Beijing Institute
MIIT Key Laboratory of Spintronics
School of Integrated Circuit Science and Engineering
Beihang University
Beijing 100191, China

H. Yu, J. Chen
Shenzhen Institute for Quantum Science and Engineering
Southern University of Science and Technology
Shenzhen 518055, China

J. Chen, D. Grundler
Laboratory of Nanoscale Magnetic Materials and Magnonics
Institute of Materials
School of Engineering
École Polytechnique Fédérale de Lausanne
STI-IMX-LMGN
Station 17, CH-1015 Lausanne, Switzerland
E-mail: dirk.grundler@epfl.ch

The ORCID identification number(s) for the author(s) of this article can be found under https://doi.org/10.1002/adfm.202203466.

V. Cros, P. Bortolotti, A. Anane
Unité Mixte de Physique CNRS, Thales
Univ Paris Sud, Université Paris Saclay
91767 Palaiseau, France

C. Guo, X. Han
Beijing National Laboratory for Condensed Matter Physics
Institute of Physics
University of Chinese Academy of Sciences
Chinese Academy of Sciences
Beijing 100190, China

F. Brandl, F. Heimbach, D. Grundler
Lehrstuhl für Physik funktionaler Schichtsysteme, Technische Universität München
Physik Department
James-Franck-Str. 1, D-85747 Garching b. München, Germany

D. Grundler
Institute of Electrical and Micro Engineering
School of Engineering
École Polytechnique Fédérale de Lausanne
Station 17, CH-1015 Lausanne, Switzerland

metasurfaces would be promising candidates for a new class of active (reconfigurable) metadevices[4,16,17] that manipulate reflected and transmitted microwave signals via spin waves and different magnetic states by modifying the external magnetic fields.

Spin waves or their quanta known as magnons can transport information free of charge flow.[18–20] They are therefore considered for low-power consuming logic devices and computing.[21–24] A magnonic metamaterial based on a single layer of nanopatterned $Ni_{80}Fe_{20}$ (permalloy) has displayed neither reconfigurable properties nor spectral filtering.[25,26] The marriage of magnonics with interface engineering and cutting-edge nanotechnology has given rebirth to the field and is expected to enable unprecedented functionalities.[27–29] Reconfigurable nanomagnonics has been realized by utilizing different spin textures[30] including magnetic domain walls[29,31–33] and magnetic vortices.[34] It was shown that nanodisks experienced symmetry breaking in the formation of vortex states due to extrinsic defects and Dzyaloshinskii–Moriya interaction (DMI) with the substrate.[35] Vortex states are topologically protected spin textures[36] and recently enabled further optimization of commercial magnetic field sensors.[37] However, all these pioneering works have not realized a metasurface which

is a recent game-changing development for on-chip wave control in photonics and plasmonics.[38] A magnetic metasurface on a low-damping ferrimagnetic insulator promises in particular reconfigurable long-distance transport of phase-coherent spin waves. The latter feature is the main asset of magnonics for signal transmission and wave-based computation at low power consumption.

Here, we demonstrate a reconfigurable ferromagnetic metasurface based on nanostructured ferromagnetic disk arrays (**Figure 1**a,b). On top of a magnonic waveguide consisting of a low damping nanometer-thick yttrium iron garnet (YIG) film, we fabricated 15 nm thick $Co_{20}Fe_{60}B_{20}$ (CoFeB), $Ni_{80}Fe_{20}$ (Py), and Co nanodisk arrays and explored their metasurface functionality at GHz frequencies. In the vortex state[39] of CoFeB nanodisks we discovered a surprisingly strong spectral filtering of microwaves when the wavelength of spin waves in YIG were about ten times larger than the period a of the nanodisk array. In this long wavelength limit $\lambda \gg a$, an effective media concept is expected to hold and describe a physical response not readily available in nature.[40] We attribute our observation to the dynamic coupling between the vortex-state resonance in the ferromagnetic nanodisks and the spin-wave excitation in the ferrimagnetic YIG (see Supporting Information).
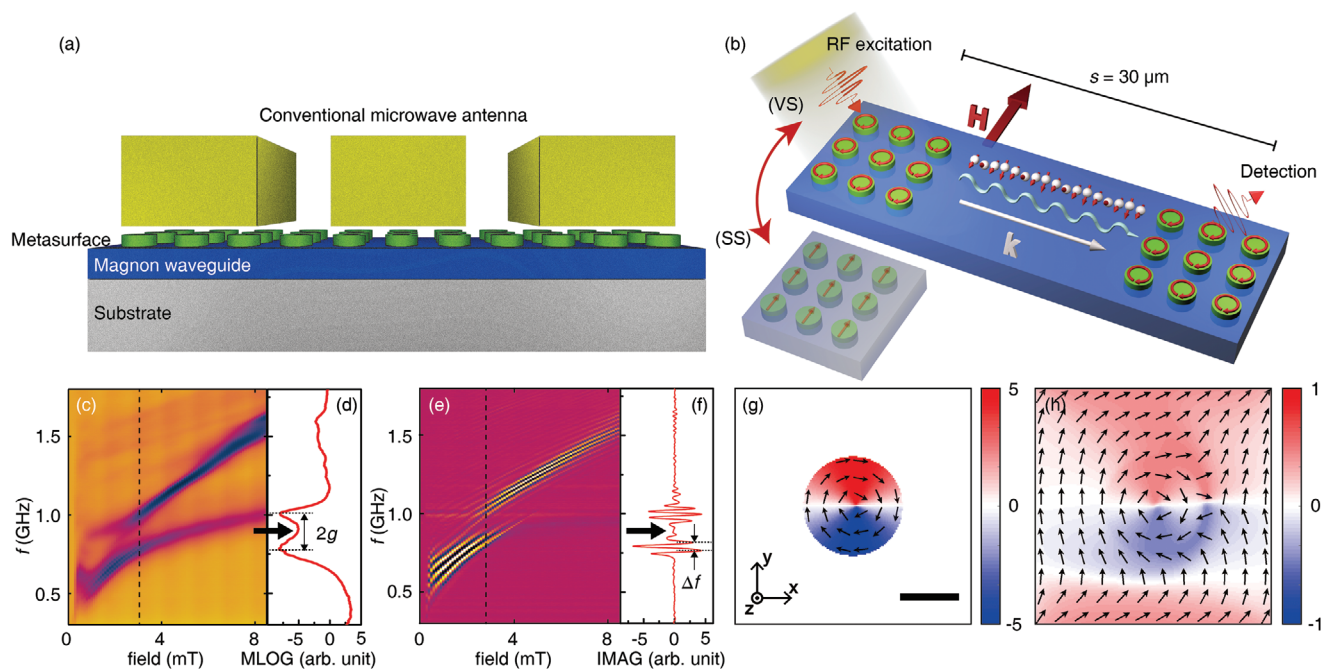
Figure 1. Reconfigurable nanomagnonic device based on ferromagnetic magnetic metasurfaces. a) Sketch of the multilayered structure, consisting of a 15 nm thick CoFeB nanodisk metasurface (green) underneath the 150 nm thick coplanar waveguide (yellow) and on top of a 20 nm thick YIG film (blue) on a 350 μm thick dielectric substrate. b) Measurement configuration. The lattice constant a amounts to 800 nm. The diameter of disks is 350 nm. Spin waves are excited by a microwave signal applied to the coplanar waveguide and detected either in reflection or transmission configuration after propagating a distance s of 30 μm. The magnetic states of the nanodisks can be switched between the vortex (VS) and saturated state (SS) for reconfigurability. c,d) Reflection spectra S_{11} taken on a single CoFeB metasurface on YIG and e,f) transmission spectra S_{21} measured for spin waves propagating between emitter and detector CPWs. The field is first set to saturation at −100 mT and then swept to positive field values. All data shown are measured with the CoFeB metasurface in the vortex state. (d) and (f) are line plots extracted from (c) and (e) at a field of 3 mT. The bold black arrows indicate the unconventional response near 0.9 GHz. g) Simulated vortex state in the CoFeB nanodisk at 2 mT applied in the plane in vertical direction. We considered periodic boundary conditions. h) Spin configuration in YIG underneath the nanodisk shown in (g). The scale bar in (g) is also valid for (h) and amounts to 350 nm. The arrows and background color display the local orientation of spins. Dark color in (c) indicates absorption (in arb. units). The signal variation in the red line spectra in (d) and (f) below 0.5 GHz reflect the noise level in the measurement. The white-black-white oscillation contrast in (e) indicates propagating spin waves (in arb. units).

**ADVANCED
SCIENCE NEWS**

www.advancedsciencenews.com

**ADVANCED
FUNCTIONAL
MATERIALS**

www.afm-journal.de

The reported metasurface functionality is reconfigured by modifying the magnetic textures via a small magnetic field. Thereby, we control long-distance spin wave transmission in a prototypical microwave delay line and induce an off/on ratio of −18.3 dB in a frequency window of 50 MHz around 0.9 GHz. The discovery of a ferromagnetic metasurface which is reprogrammed via topologically protected vortex states enables unprecedented electromagnetic wave manipulation which goes beyond its nonmagnetic counterparts explored in photonics and plasmonics.

2. Results and Discussions

2.1. Reconfigurable Ferromagnetic Magnetic Metasurfaces

Figure 1a shows a sketch of the multilayered structure incorporating a layer of ferromagnetic nanodisks which give rise to the metasurface functionality. The nanodisks were fabricated from amorphous CoFeB (and polycrystalline Py or Co) with a thickness of 15 nm on 20-nm-thick YIG. The disks exhibited a diameter of 350 ± 5 nm and were arranged on a square lattice with a lattice constant of $a = 800$ nm. Two identical coplanar waveguides (CPWs) were integrated and separated by 30 µm (center-to-center separation) to form a microwave delay line. The CPWs covered the nanodisks to inject and detect the microwave signals in YIG via the metasurface (Figure 1b). An external field H was applied in the plane of the nanodisks and perpendicular to the spin wave vector k provided by the emitter CPW. It is known that a metasurface response can be obtained in a hybrid structure in which a certain resonance couples strongly to a different fundamental excitation.[41] To study such coupling in our samples, we used a broadband spin-wave spectroscopy setup based on a vector network analyzer (VNA).[42] The VNA generated a radiofrequency magnetic field in the emitter CPW that exerted a torque on the underlying spins. We measured reflection and transmission signals as a function of field H via scattering parameters S_{11} (Figure 1c,d) and S_{21} (Figure 1e,f), respectively. When measuring S_{21} the microwave signal was transmitted by spin waves through the thin YIG along a macroscopic path with a length of 23 µm. We note that in bare YIG large transmission signals can occur if i) the microwave frequency f resides within the allowed magnon band as given by the dispersion relation $f(k)$[43] and ii) the emitter CPW provides appropriate wavevectors k.[44] In this work we focus on an allowed magnon band in YIG mainly between 0.85 and 0.95 GHz which is covered by our CPWs. The CPWs provide the relevant excitation strength and wavevector distribution around 0.8 rad µm^{-1} (see Supporting Information).
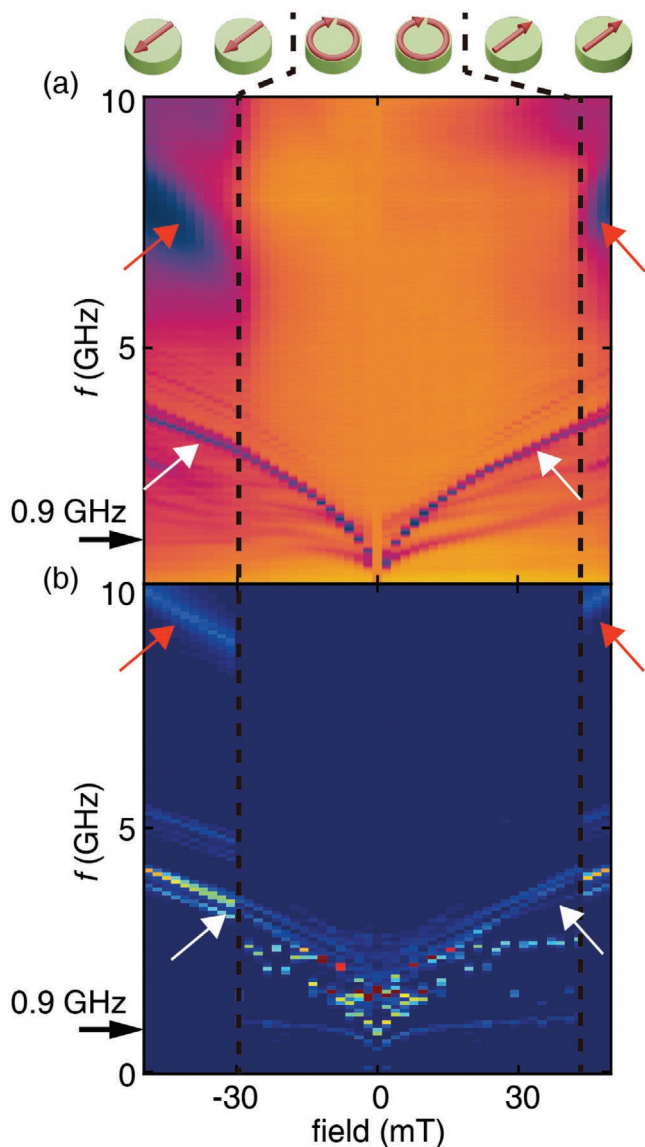
In Figure 1c,f, all data were obtained in the vortex state of CoFeB nanodisks (Figure 1g). The bold black arrow of Figure 1f highlights a severe and unexpected signal suppression (see Supporting Information). The corresponding spectral filtering in our multilayered sample at 0.9 GHz is unconventional and counterintuitive as the relevant CPW has its maximum excitation strength in YIG just near this frequency at 3 mT. The corresponding minimum in absorption (black arrow in Figure 1d) cannot be explained by a magnonic crystal band gap at the Brillouin zone (BZ) boundary of the periodic lattice.

The BZ boundary corresponds to a wavevector $k_{BZ} = \pi/a = 3.93$ rad µm^{-1} which in YIG would correspond to a frequency of roughly 1.3 GHz at 3 mT. This is outside the considered frequency regime. Following the spin-wave dispersion relation of 20 nm thick YIG (see Supporting Information) the frequency $f = 0.9$ GHz corresponds to a wavelength of 8.06 µm. This value is much larger than the lattice constant a and the observed signal filtering is hence attributed to a metasurface property of the nanodisk array. In the following we investigate the resonances which couple in our multilayered sample and, in Figure 1c, undergo an avoided crossing (anticrossing) as a function of H.

2.2. Reflection Spectra at Vortex and Saturate States

Color-coded reflection spectra S_{22} were taken over a broad field regime and are displayed in **Figure 2**a. Below −30 mT (marked by the left dashed vertical line) and above 45 mT (marked by the right dashed vertical line) pronounced branches of absorption are observed at high frequencies (orange arrows). For such magnetic fields the nanodisks are saturated, and the pronounced high-frequency branches are attributed to their center mode of spin-precessional motion. For smaller absolute field values (i.e., in the field regime between the two vertical lines) these high-frequency branches are absent suggesting the nanodisks to be in a different magnetic state. The branches of large absorption highlighted by white arrows do not vanish at the fields marked by vertical lines. They are attributed to spin wave resonances in the soft-magnetic YIG consistent with branches seen in ref. [42]. Since the saturation magnetization M_S of YIG is much smaller than M_S of CoFeB, spin-precessional motion in saturated YIG exhibits a smaller frequency than the saturated CoFeB nanodisks. The branches observed below the YIG mode in large absolute fields are attributed to magnonic crystal modes. In small fields of only a few mT we observe numerous absorption features which reside at frequencies smaller than about 1.5 GHz. Near 0.9 GHz (horizontal arrow) a resonance is seen which exhibits a very small agility df/dH at −15 mT.

In Figure 2b we show simulated spectra for which we assumed a vortex state in CoFeB nanodisks (Figure 1g) between the vertical broken lines and a saturated state otherwise (compare illustration on the top of Figure 2a). The simulations provide branches (bright) whose frequencies and field dependencies are consistent with the experimental observations described above. The simulations remodel the branches attributed to excitation in the thin YIG film (white arrows) and the high-frequency excitations in the saturated nanodisks (orange arrows). Consistent with our experiment the simulations contain a specific branch near 0.9 GHz (horizontal arrow) whose agility df/dH is almost zero at − 15 mT. Based on further simulations (see Supporting Information) we find that this low-frequency branch reflects the spin-precessional motion in CoFeB nanodisks when they are in the vortex state. When varying the field, the vortex core moves but is topologically stabilized inside the disk.[37] In Figure 2b this branch has a mirror-symmetric counterpart at positive field. In the experiment of Figure 2a the slopes df/dH at negative and positive fields are slightly different (see Supporting Information) and will be discussed below. Note

**ADVANCED
SCIENCE NEWS**

www.advancedsciencenews.com

**ADVANCED
FUNCTIONAL
MATERIALS**

www.afm-journal.de

Figure 2. Reflection spectra at different magnetic states: experiments versus simulations. a) Reflection spectra S_{22} measured when magnetic field is swept from negative saturation. Dark color indicates resonance absorption (in arb. units). The statistical noise can be seen in the field-independent background signal level. The applied field was initially set to −100 mT and then swept from −50 to 50 mT with a step of 2 mT. For each external magnetic field, VNA measures a single spectrum of S_{22} with frequency band from 10 MHz to 10 GHz. The black dashed lines separate the saturation state and vortex state of the CoFeB nanodisks. b) Results from micromagnetic simulations where the metasurface is set to switch from saturated state to vortex state and vice versa at the vertical lines. In (a) and (b) the horizontal black arrow indicates a branch of small agility df/dH which we attribute to the spin-precessional resonance in the CoFeB nanodisks when in the vortex state (Figure S1b, Supporting Information). Bright color in (b) indicate spin-precessional motion (in arb. units). The field-independent scatter in data points and brightness reflect the statistical error.

that our simulations consider neither extrinsic defects nor DMI and assume a homogeneous excitation.

Following the simulations, the feature marked by bold black arrows in Figure 1d,f resides in the frequency region where the

vortex excitation of individual CoFeB nanodisks is degenerated with spin-wave excitations near k_1 in YIG. In the multilayered sample these excitations are coupled and undergo an avoided crossing (anticrossing). Correspondingly a local minimum is observed in the absorption curve (arrow in Figure 1d). We note that below 3 mT we observe a faint branch in Figure 1c that follows the resonance mode known from bare YIG. We attribute the weak signal to the unpatterned YIG film underneath the edges of the CPW. This observation further substantiates our interpretation that the anticrossing gap reflects an avoided crossing between the field-dependent (agile) YIG resonance and the almost constant nanodisk mode (see Supporting Information). Though the avoided crossing does not generate an absolute minimum in the absorption of Figure 1d, it leads to a significant spectral filtering at 0.9 GHz and thereby to an almost complete suppression of the spin-wave propagation signal between the two CPWs in Figure 1f (arrow). Note that the spin wave modes which propagate with frequencies close to the anticrossing gap are not significantly modified. We extracted their group velocities v_g from the transmission spectra of S_{12} according to ref. [42]

$$v_g = \frac{\partial \omega}{\partial k} = \Delta f \times s \tag{1}$$

where Δf is the frequency separation extracted from S_{12} spectra, as shown in Figure 1f, and $s = 30$ μm. The group velocities below and above the gap at 3 mT are about 1.6 km s^{-1} and 1.3 km s^{-1} respectively, comparable to v_g of bare YIG. Note that branch degeneracies (crossings) reported for high frequencies in the limit of $\lambda \leq a$ (periodic media concept) in ref. [45] led to an enhanced signal strength of propagating spin waves in YIG. The metasurface performance reported here is of opposite functionality and leads to an efficient suppression via spectral filtering.

2.3. Spectral Filtering Functionality Based on the Magnetic Metasurface

In **Figure 3**a we show the spin-wave propagation signal measured on bare YIG without nanodisks. We observe a peak-to-peak signal Δ_b of 16.2 near 0.9 GHz. In Figure 3b we replot the data from Figure 1f on the same scales for direct comparison and find $\Delta_{off} = 0.35$ in the yellow shaded frequency regime. The ratio Δ_{off}/Δ_b amounts to 0.022 (2.2%) in a frequency band of about 50 MHz. The corresponding ratio for absorption is $\Gamma_{off}/\Gamma_b = 0.39$ (39%). The coverage by CoFeB nanodisks alone cannot explain the strikingly different performance of the two samples. It amounts to only 15% of the interfacial area between CPW and YIG, that is, 85% of the YIG is exposed directly to microwave excitation. The efficient signal filtering in YIG is not attributed to the physical properties of the natural material CoFeB (see Supporting Information).

In the following we discuss the metasurface property and magnetic coupling between nanodisks and YIG. The coupling strength g is defined as half of the minimal peak-to-peak frequency spacing in the avoided crossing of Figure 1c.[46–48] At 3 mT, we extract $g = 0.11 \pm 0.003$ GHz. From our simulations
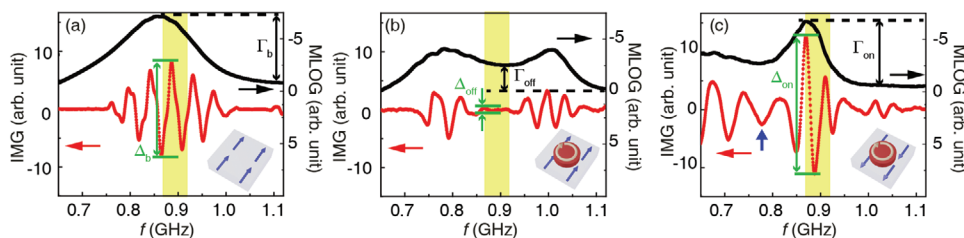
Figure 3. Realization of spectral filtering based on the magnetic metasurface. a) Reflection (S_{11}, black) and transmission (S_{21}, red) spectra obtained at +3 mT on a bare 20 nm thick YIG film. The resonance in the magnitude (MLOG) of S_{11} and its linewidth reflect the wavevector k_1 and the wavevector distribution, respectively, provided by the exciting CPW. The oscillating signal in the imaginary (IMG) part of S_{21} indicates propagating spin waves between two CPWs. Reflection and transmission spectra with an applied field of b) −1.5 mT and c) +3 mT measured on YIG containing the metasurface. In all graphs the frequency regime ranging from 0.87 to 0.92 GHz is highlighted by yellow shading. The samples possessed nominally identical CPWs. The parameters Γ_i and Δ_i (with i = b, on, off) are used to extract and compare the signal strengths related to the shaded frequency regime in all graphs. The upward arrow in (c) indicates a decrease in amplitude which we attribute to an avoided crossing occurring outside the yellow-shaded region. The scales of the y-axes are the same in (a) to (c) and are without units as the displayed curves (spectra) reflect scattering parameters measured in dB (here presented on the linear scale). The statistical background noise level of the setup can be seen in the red and black curves of (a) between 0.65 and 0.75 GHz.

we find that exchange coupling between CoFeB and YIG is key to remodel the observed spectra. It induces a non-collinear spin structure in YIG just underneath the nanodisks (Figure 1h). Combined with the dipolar interaction, the exchange coupling explains the relatively large g value. In the experiment we observe that the low-frequency branches and corresponding avoided crossings are not fully mirror symmetric with respect to H = 0. At −1.5 mT (Figure 3c) the induced gap (blue arrow) is shifted such that we obtain a large transmitted spin wave signal in the yellow shaded frequency regime. We attribute this gap shift to an asymmetric behavior of the vortex mode at positive and negative magnetic fields. It could result from extrinsic defects or DMI.[35] DMI occurs due to lack of inversion symmetry near the surface of the nanodisk array and CoFeB growth on an oxide.[49] We find a signal strength Δ_{on} in Figure 3c which is a factor of 68 larger compared to Δ_{off} in Figure 3b. The observed symmetry enables a reconfigurable metasurface with spectral filtering capability (efficiency) of hence −18.3 dB (98.5%) between Δ_{on} and Δ_{off}. We note that Γ_{off} (absorption) is smaller than Γ_{on} by only −3.9 dB. Pronounced absorption still
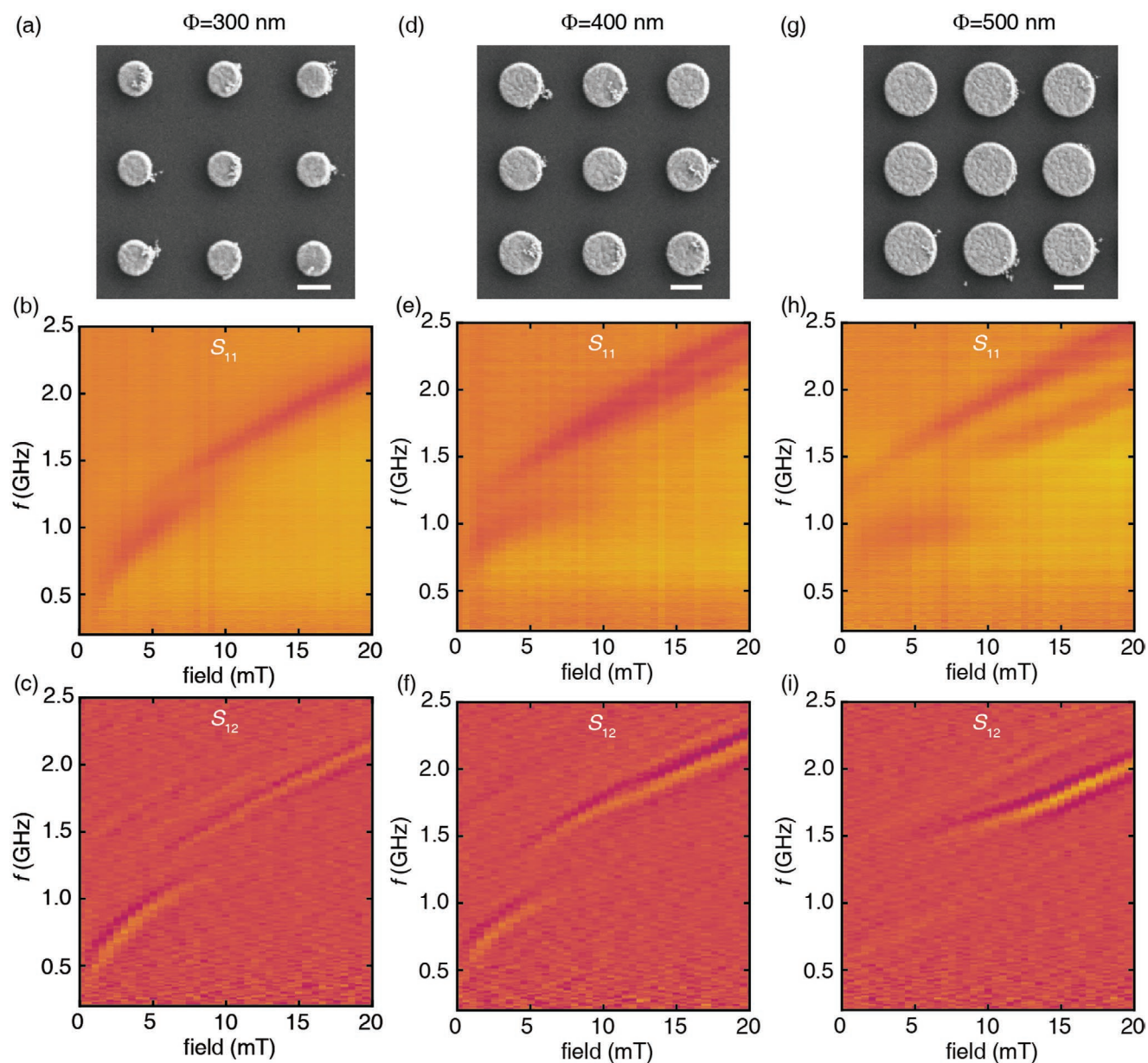
takes place, but coupling of the microwave signal to the propagating mode in YIG is efficiently blocked.

2.4. Material Dependence of the Spectra Filtering Function

Now we investigate the material dependence of the spectral filtering functionality. In **Figure 4** (**Figure 5**) we report on samples for which we replaced CoFeB by Py (Co). Py exhibited $\mu_0 M_S$ = 1.0 T compared to 1.8 T in case of CoFeB. We followed the same measurement protocol as used for Figure 1c–f. The color-coded reflection and transmission spectra taken in the vortex state of Py nanodisks are shown in Figure 4a and c, respectively. Individual lineplots extracted at 4.2 mT are shown in Figure 4b,d. An avoided crossing with a magnetic coupling strength of g = 0.06 ± 0.007 GHz is found. The propagating spin wave signal is suppressed at the anticrossing gap. Here the suppression corresponds to −7.0 dB and is considerably weaker than for the CoFeB-based metasurface. To compare the two metasurfaces we consider the cooperativity[48]
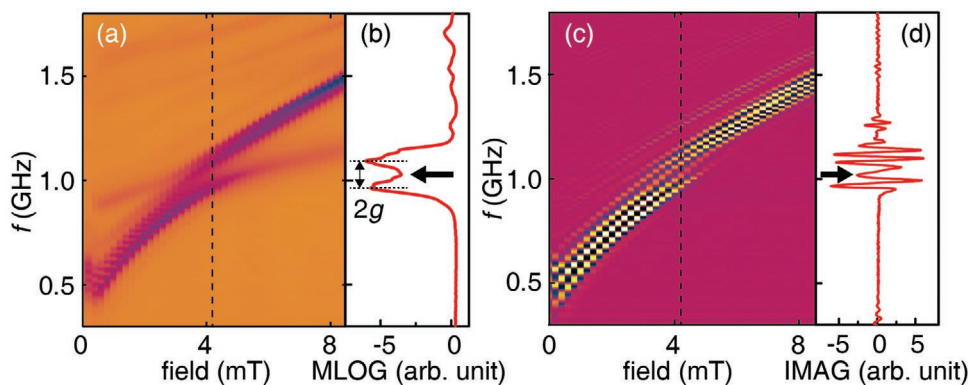
Figure 4. Reconfigurable nanomagnonic device based on Py metasurfaces. a) Reflection spectra S_{11} and c) transmission spectra S_{12} are measured in the Py metasurface based nanomagnonic device. The field is first set to saturation at −100 mT and then swept to positive field values. All data shown are measured with the Py metasurface in the vortex state. (b) and (d) are line plots extracted from (a) and (c) at 4.2 mT (dashed lines). Arrows highlight the avoided crossing. Dark color in (a) indicates absorption (in arb. units). The signal variation in the red line spectra in (b) and (d) between 0.5 and below 0.8 GHz reflect the noise level in the measurement. The white-black-white oscillation contrast in (c) indicates propagating spin waves (in arb. units).

**ADVANCED
SCIENCE NEWS**

www.advancedsciencenews.com

**ADVANCED
FUNCTIONAL
MATERIALS**

www.afm-journal.de

Figure 5. Transmission and reflection spectra of three hybrid devices with magnetic nanodisks of different diameters ϕ. a,d,g) Scanning electron microscopy (SEM) images of three metasurface devices with $\phi = 300$ nm, 400 nm, and 500 nm, respectively. b,c) Reflection spectra S_{11} and transmission spectra S_{12} of the device with $\phi = 300$ nm. e,f) Reflection spectra S_{11} and transmission spectra S_{12} of the device with $\phi = 400$ nm. h,i) Reflection spectra S_{11} and transmission spectra S_{12} of the device with $\phi = 500$ nm. The scale bars indicate 300 nm. In the central row dark color indicates absorption (in arb. units). Horizontal and vertical stripes indicate the remaining noise in the setup. In the bottom row the white-black-white oscillating contrast indicates propagating spin waves (in arb. units). The field-independent background noise level is directly visible in the color-coded spectra.

$$C = g^2 \left(\kappa_m^{\text{Vortex}} \times \kappa_m^{\text{YIG}} \right)^{-1} \qquad (2)$$

where $\kappa_m^{\text{Vortex}} \approx 0.082$ GHz for CoFeB ($\kappa_m^{\text{Vortex}} \approx 0.069$ GHz for Py) and $\kappa_m^{\text{YIG}} \approx 0.031$ GHz are the dissipation rates extracted from the half-width at half-maximums of the two crossing branches in the investigated devices. In case of CoFeB we find $g > \kappa_m^{\text{Vortex}}, \kappa_m^{\text{YIG}}$ and a cooperativity $C = 4.7$. This value is much larger than both $C = 0.38$ reported recently for Ni nanostripes exchange-coupled to YIG[48] and $C = 1.7$ extracted for the Py

metasurface. Our results show that a large cooperativity C (i.e., coupling), is important to obtain an efficient filtering. A large value of C (Equation (2)) is ensured by a large gap $2g$ and, preferentially, small κ_m^{YIG}, that is, a long magnon lifetime in YIG. This combination of parameters provides a reconfigurable metasurface with a large on/off ratio. Our comparison of different ferromagnets suggests that the high saturation magnetization of CoFeB induces a larger gap $2g$ compared to Py (and Ni). We attribute the improved performance to an enhanced interlayer coupling by stronger dipolar interaction. Still we found that the

metasurface based on Py provided an additional means of controllability in that both the vortex and the saturated state existed at small magnetic field (see Supporting Information).

To enhance the signal suppression by spectral filtering one might consider a larger surface coverage of vortex-containing nanostructures. Figure 5 shows the microwave reflection and transmission spectra of three Co-based metasurface devices on YIG with the Co nanodisk diameters ϕ of 300, 400, and 500 nm. The periods of the metasurfaces are fixed at the same value of 800 nm. Two CPWs are patterned on top of two opposing Co nanodisk arrays with the center-to-center distance of 12 µm and plain YIG in-between. Figure 5b,e,h shows reflection spectra with different Co nanodisk diameters. We observe that the anticrossing gap increases with increasing diameter of the Co nanodisks. The anticrossings appear at around 1.2 GHz which is a little higher than that in the CoFeB-based metasurface. This might be explained by the different dipolar interaction and magnetocrystalline anisotropy in Co grains. Transmission spectra in Figure 5c,f,i clearly show the spectral filtering function in the Co-based metasurface devices. Similar to the reflection spectra, the spectral filtering band enlarges with increasing diameter of the Co nanodisks. We attribute this observation to the increasing interface area and interlayer magnetic coupling.

3. Conclusion

We note that the significant spectral filtering by about −18 dB was achieved by means of 15-nm-thin CoFeB nanodisks covering only 15% of the relevant antenna surface with a lattice constant of 800 nm. To achieve the same suppression of about -20 dB via a magnonic crystal and the corresponding periodic media concept, the authors of ref. [50] needed to prepare 1700 nm deep grooves in 5.5 µm thick YIG. For a magnonic crystal with a period of 30 µm in 260 nm thick YIG a filtering by −13 dB was achieved by 4000 nm wide grooves filled with 260 nm thick CoFeB.[51] The CoFeB metasurface reported here is thinner by more than an order of magnitude, more compact, filters more efficiently and requires much less materials resources compared with the periodic media concept. The metasurface functions in the long-wavelength limit $\lambda \gg a$, with the wavelength of the relevant spin wave being ten times larger than the nanodisk period. Hence distances between vortex-hosting disks are deep-subwavelength. The wave interference or scattering reported in ref. [52] cannot explain the wave phenomena we observe. Skyrmion lattices consisting of nanoscale spin whirls might provide an alternative for ultracompact magnetic metasurfaces. In their case magnetoelectric coupling[53] offers further control parameters. At the same time higher operational frequencies could be reached.[54,55] Interfacially induced skyrmions promise the creation of ferromagnetic metasurfaces on curved topographies.[56,57]

In conclusion we report the discovery of a reconfigurable ferromagnetic metasurface in a prototypical microwave delay line. We thereby demonstrate a unique method to control long distance spin wave propagation with a high on/off ratio at a specific frequency band. Exploiting the effective media concept, the pass band loss of the YIG magnonic channel is not deteriorated. This is a significant performance gain compared to filters based on magnonic crystals following the periodic media concept. The

reconfigurable metasurface offers hence advanced functionality for magnon spintronics and on-chip microwave devices.

4. Experimental Section

Device Fabrication: The YIG thin films were grown on Gadolinium Gallium Garnet (111) substrate using pulsed laser deposition by a temperature of 650 degree Celsius and an oxygen pressure of 0.25mbar. The film thickness was determined by X-ray reflectometry to be 20 nm and the RMS roughness was found to be better than 0.5 nm. The Gilbert damping parameter was determined to be around 2.3×10^{-4}. It was then shaped by lithography and ion beam etching to be a 300 µm wide strip. Afterward electron beam lithography and lift-off processing were used to prepare nanodisk arrays with diameters of 350 ± 5 nm and a lattice constant of 800 nm on YIG film. The nanodisks were fabricated by magnetron sputtering of amorphous $Co_{20}Fe_{60}B_{20}$ or evaporation of polycrystalline $Ni_{80}Fe_{20}$ or Co with a thickness of 15 nm. The spin waves were excited and detected by coplanar waveguides (CPWs) integrated on top of the nanodisks region. The distance between the centers of the two CPW signal lines was 30 µm. The CPWs consisted of 150 nm thick Au and thin Cr as an adhesion layer. They were designed with 2.1-µm-wide signal and ground lines, and 1.4-µm-wide gaps between them. Note that the nanodisk arrays resided only at the excitation and detection regions. The region in between consisted of unpatterned YIG film, as shown in Figure 1a.

Microwave Spectroscopy: For microwave spectroscopy on the CoFeB/YIG, $Ni_{80}Fe_{20}$/YIG, and Co/YIG hybrid structures a setup based on a vector network analyzer was used, which covered a frequency regime from 10 MHz to 26.5 GHz. Impedance-matched microwave cables and microwave probes were used to connect the VNA ports with the coplanar waveguides integrated on top of YIG. Using two ports scattering parameters were measured in reflection and transmission configuration. The sample resided between a 2D vector magnet allowing to apply in-plane magnetic fields up to about 100 mT in different directions. Here results are discussed for which the magnetic field H was applied perpendicular to the spin wave wavevector k. Hence Damon–Eschbach spin waves were studied, if not otherwise specified. Further details about the CoFeB/YIG hybrid structure and VNA spectra can be found in ref. [45]. There, an independent phenomenon was discussed, that is, the grating coupler effect near 10 GHz, far outside the frequency regime considered here. In case of the grating coupler, the relevant wavelength λ of spin waves in YIG was 88 nm and shorter by about a factor of 9 compared to the lattice constant a. Under such a condition $\lambda \leq a$, Bragg reflection, Bloch theorem and periodic media concepts[40] were relevant to understand wave properties. However, in the present paper the discovery of an unconventional response in a completely different wavelength regime was reported. The metasurface effect discussed here occurred pronouncedly near 0.9 GHz (see Supporting Information) where λ in YIG was about 8 µm and 10 (100) times larger than a (in ref. [45]). In this long wavelength limit $\lambda \gg a$, an effective media concept held and described a physical response not readily available in nature.[40]

Micromagnetic Simulations: The micromagnetic simulation was performed by program OOMMF (http://math.nist.gov/oommf). For the parameters of magnetic materials, a saturation magnetization $M_S = 140$ kA m^{-1}, an exchange constant $A = 3.7 \times 10^{-12}$ J m^{-1}, and a damping coefficient $\alpha = 2.3 \times 10^{-4}$ were used for YIG and $M_S = 1430$ kA m^{-1}, $A = 28 \times 10^{-12}$ J m^{-1}, and $\alpha = 1 \times 10^{-2}$ were used for CoFeB. The exchange coefficient between YIG and CoFeB nanodisk was set to $A = 1 \times 10^{-12}$ J m^{-1}. No interlayer was set between YIG and CoFeB. The simulated structure consisted of YIG film (0.8 µm × 0.8 µm × 0.02 µm) (*xyz*) and CoFeB nanodisk with a diameter of 0.35 µm and a thickness of 0.02 µm on top of YIG. No interlayer was set between YIG and CoFeB. The cell sizes of the simulated structure were 5 nm × 5 nm × 5 nm. 2D periodical boundary condition was included in the simulation. The magnetization oscillations were excited by a uniform field in x direction with $\mu_0 H = 2$ mT according to a sine cardinal (sinc) function. The external magnetic field was applied in y direction. The simulation was performed for 200 times with the time step of 5 ps. A fast

Fourier transformation (FFT) was performed in x direction according to the acquired magnetization components.

Statistical Analysis: All data were analyzed using MATLAB (MathWorks). All data were presented as mean ± standard deviation (SD). Five independent devices were fabricated and measured, and all show similar performance.

Supporting Information

Supporting Information is available from the Wiley Online Library or from the author.

Conflict of Interest

The authors declare no conflict of interest.

Data Availability Statement

The data that support the findings of this study are available from the corresponding author upon reasonable request.

[1] N. Yu, F. Capasso, *Nat. Mater.* **2014**, *13*, 139.
[2] G. Yoon, T. Tanaka, T. Zentgraf, J. Rho, *J. Phys. D: Appl. Phys.* **2021**, *54*, 383002.
[3] S. B. Glybovski, S. A. Tretyakov, P. A. Belov, Y. S. Kivshar, C. R. Simovski, *Phys. Rep.* **2016**, *634*, 1.
[4] T. Cui, B. Bai, H.-B. Sun, *Adv. Funct. Mater.* **2019**, *29*, 1806692.
[5] A. Leitis, A. Heßler, S. Wahl, M. Wuttig, T. Taubner, A. Tittl, H. Altug, *Adv. Funct. Mater.* **2020**, *30*, 1910259.
[6] A. A. High, R. C. Devlin, A. Dibos, M. Polking, D. S. Wild, J. Perczel, N. P. de Leon, M. D. Lukin, H. Park, *Nature* **2015**, *522*, 192.
[7] G. Ma, M. Yang, S. Xiao, Z. Yang, P. Sheng, *Nat. Mater.* **2014**, *13*, 873.
[8] V.S. Asadchy, I.A. Faniayeu, Y. Ra'di, S.A. Khakhomov, I.V. Semchenko, S.A. Tretyakov, *Phys. Rev. X* **2015**, *5*, 031005.
[9] T. Han, K. Wen, Z. Xie, X. Yue, *Prog. Electromagn. Res.* **2022**, *173*, 1.
[10] Z. Li, G. Cao, C. Li, S. Dong, Y. Deng, X. Liu, J. S. Ho, C. Qiu, *Prog. Electromagn. Res.* **2021**, *171*, 1.
[11] M. R. D. Kodnoeih, Y. Letestu, R. Sauleau, E. M. Cruz, A. Doll, *IEEE Antennas Wireless Propag. Lett.* **2018**, *17*, 873.
[12] N. Bonod, *Nat. Mater.* **2015**, *14*, 664.
[13] C. Qian, B. Zheng, Y. Shen, L. Jing, E. Li, L. Shen, H. Chen, *Nat. Photonics* **2020**, *14*, 383.
[14] Y. Zheng, K. Chen, W. Yang, L. Wu, K. Qu, J. Zhao, T. Jiang, Y. Feng, *Adv. Funct. Mater.* **2022**, *32*, 2107699.
[15] J. Lähnemann, V. M. Kaganer, K. K. Sabelfeld, A. E. Kireeva, U. Jahn, C. Chèze, R. Calarco, O. Brandt, *Phys. Rev. Appl.* **2022**, *17*, 024019.
[16] N. I. Zheludev, Y. S. Kivshar, *Nat. Mater.* **2012**, *11*, 917.
[17] Y. Huang, H. W. H. Lee, R. Sokhoyan, R. A. Pala, K. Thyagarajan, S. Han, D. P. Tsai, H. A. Atwater, *Nano Lett.* **2016**, *16*, 5319.
[18] B. Lenk, H. Ulrichs, F. Garbs, M. Münzenberg, *Phys. Rep.* **2011**, *507*, 107.
[19] S. Neusser, D. Grundler, *Adv. Mater.* **2009**, *21*, 2927.
[20] A. V. Chumak, V. I. Vasyuchka, A. A. Serga, B. Hillebrands, *Nat. Phys.* **2015**, *11*, 453.
[21] G. Csaba, A. Papp, W. Porod, *Phys. Lett. A* **2017**, *381*, 1471.
[22] L. J. Cornelissen, J. Liu, R. A. Duine, J. B. Youssef, B. J. van Wees, *Nat. Phys.* **2015**, *11*, 1022.
[23] R. Lebrun, A. Ross, S. A. Bender, A. Qaiumzadeh, L. Baldrati, J. Cramer, A. Brataas, R. A. Duine, M. Kläui, *Nature* **2018**, *561*, 222.
[24] A. Khitun, K. L. Wang, *Superlattices Microstruct.* **2005**, *38*, 184.
[25] S. Neusser, G. Duerr, S. Tacchi, M. Madami, M. L. Sokolovskyy, G. Gubbiotti, M. Krawczyk, D. Grundler, *Phys. Rev. B* **2011**, *84*, 094454.
[26] S. Neusser, H. G. Bauer, G. Duerr, R. Huber, S. Mamica, G. Woltersdorf, M. Krawczyk, C. H. Back, D. Grundler, *Phys. Rev. B* **2011**, *84*, 184411.
[27] H. Yu, G. Duerr, R. Huber, M. Bahr, T. Schwarze, F. Brandl, D. Grundler, *Nat. Commun.* **2013**, *4*, 2702.
[28] A. Haldar, D. Kumar, A. O. Adeyeye, *Nat. Nanotechnol.* **2016**, *11*, 437.
[29] K. Wagner, A. Kákay, K. Schultheiss, A. Henschke, T. Sebastian, H. Schultheiss, *Nat. Nanotechnol.* **2016**, *11*, 432.
[30] E. Albisetti, D. Petti, G. Sala, R. Silvani, S. Tacchi, S. Finizio, S. Wintz, A. Calò, X. Zheng, J. Raabe, E. Riedo, R. Bertacco, *Commun. Phys.* **2018**, *1*, 56.
[31] S. J. Hämäläinen, M. Madami, H. Qin, G. Gubbiotti, S. van Dijken, *Nat. Commun.* **2018**, *9*, 4853.
[32] V. Sluka, T. Schneider, R. A. Gallardo, A. Kákay, M. Weigand, T. Warnatz, R. Mattheis, A. Roldán-Molina, P. Landeros, V. Tiberkevich, A. Slavin, G. Schütz, A. Erbe, A. Deac, J. Lindner, J. Raabe, J. Fassbender, S. Wintz, *Nat. Nanotechnol.* **2019**, *14*, 328.
[33] L. Chang, Y. Liu, M. Kao, L. Tsai, J. Liang, S. Lee, *Sci. Rep.* **2018**, *8*, 3910.
[34] S. Wintz, V. Tiberkevich, M. Weigand, J. R. , J. Lindner, A. Erbe, A. Slavin, J. Fassbender, *Nat. Nanotechnol.* **2016**, *11*, 948.
[35] M. Im, P. Fischer, K. Yamada, T. Sato, S. Kasai, Y. Nakatani, T. Ono, *Nat. Commun.* **2012**, *3*, 983.
[36] H. B. Braun, *Adv. Phys.* **2012**, *61*, 1.
[37] D. Suess, A. Bachleitner-Hofmann, A. Satz, H. Weitensfelder, C. Vogler, F. Bruckner, C. Abert, K. Prügl, J. Zimmer, C. Huber, S. Luber, W. Raberg, T. Schrefl, H. Brückl, *Nat. Electr.* **2018**, *1*, 362.
[38] A. S. Solntsev, G. S. Agarwal, Yu.s. Kivshar, *Nat. Photonics* **2021**, *15*, 327.
[39] T. Shinjo, T. Okuno, R. Hassdorf, K. Shigeto, T. Ono, *Science* **2000**, *289*, 930.
[40] N. Engheta, R. W. Ziolkowski, *Metamaterials – Physics and Engineering Explorations*, John Wiley & Sons, Hoboken, NJ **2006**.
[41] O. Wolf, S. Campione, J. Kin, I. Brener, *Opt. Express* **2016**, *24*, 21512.
[42] H. Yu, O. d'Allivy Kelly, V. Cros, R. Bernard, P. Bortolotti, A. Anane, F. Brandl, R. Huber, I. Stasinopoulos, D. Grundler, *Sci. Rep.* **2014**, *4*, 6848.

[43] B. A. Kalinikos, A. N. Slavin, *J. Phys. C Solid State Phys.* **1986**, *19*, 7013.

[44] S. Maendl, I. Stasinopoulos, D. Grundler, *Appl. Phys. Lett.* **2017**, *111*, 012403.

[45] H. Yu, O. d' Allivy Kelly, V. Cros, R. Bernard, P. Bortolotti, A. Anane, F. Brandl, F. Heimbach, D. Grundler, *Nat. Commun.* **2016**, *7*, 11255.

[46] H. Huebl, C. W. Zollitsch, J. Lotze, F. Hocke, M. Greifenstein, A. Marx, R. Gross, S. T. B. Goennenwein, *Phys. Rev. Lett.* **2013**, *111*, 127003.

[47] X. Zhang, C.-L. Zou, L. Jiang, TangH. X , *Phys. Rev. Lett.* **2014**, *113*, 156401.

[48] J. Chen, C. Liu, T. Liu, Y. Xiao, K. Xia, G. E. W. Bauer, M. Wu, H. Yu, *Phys. Rev. Lett.* **2018**, *120*, 217202.

[49] B. Dieny, M. Chshiev, *Rev. Mod. Phys.* **2017**, *89*, 025008.

[50] A. V. Chumak, A. A. Serga, S. Wolff, B. Hillebrands, M. P. Kostylev, *Appl. Phys. Lett.* **2009**, *94*, 172511.

[51] H. Qin, G. Both, S. J. Hämäläinen, L. Yao, S. van Dijken, *Nat. Commun.* **2018**, *9*, 5445.

[52] J. Förster, J. Gräfe, J. Bailey, S. Finizio, N. Träger, F. Groß, S. Mayr, H. Stoll, C. Dubs, O. Surzhenko, N. Liebing, G. Woltersdorf, J. Raabe, M. Weigand, G. Schütz, S. Wintz, *Phys. Rev. B* **2019**, *100*, 214416.

[53] S. Seki, S. Ishiwata, Y. Tokura, *Phys. Rev. B* **2012**, *86*, 060403.

[54] T. Schwarze, J. Waizner, M. Garst, A. Bauer, I. Stasinopoulos, H. Berger, C. Pfleiderer, D. Grundler, *Nat. Mater.* **2015**, *14*, 478.

[55] E. Turgut, M. J. Stolt, S. Jin, G. D. Fuchs, *J. Appl. Phys.* **2017**, *122*, 183902.

[56] V. P. Kravchuk, U. K. Rößler, O. M. Volkov, D. D. Sheka, J. van den Brink, D. Makarov, H. Fuchs, H. Fangohr, Y. Gaididei, *Phys. Rev. B* **2016**, *94*, 144402.

[57] X. Wang, X. Wang, C. Wang, H. Yang, Y. Cao, P. Yan, *J. Phys. D: Appl. Phys.* **2019**, *52*, 225001.